A Multi-Vehicle, Multi-Lane Cooperative Driving Framework in Mixed Traffic with Driving Advisory

Sanzida Hossain[1], *Student Member, IEEE*, Jiaxing Lu[2], *Student Member, IEEE*, He Bai[1], *Member, IEEE* and Weihua Sheng[2], *Senior Member, IEEE*

***Abstract*—In a mixed-traffic environment, where autonomous vehicles (AVs) and human-driven vehicles are operating side by side, cooperative driving can become a useful tool to facilitate safe coordination. Unlike AVs, human-driven vehicles are difficult to model and control. Existing literature is largely focused on collaboration between AVs considering human vehicles as obstacles or unconnected and uncontrollable entities. In this paper, we present a cooperative driving framework that actively influences human-driven vehicles via advising commands and enables them to cooperate with AVs to achieve coordinated driving behaviors. We formulate cooperative driving as a stochastic model predictive control (sMPC) problem and consider human drivers' various stochastic aspects, such as attentiveness and tendency to follow an advisory action. The solutions to the sMPC provide advisory for longitudinal actions and lane change to human-driven vehicles and control commands to autonomous vehicles. With simulation and human-in-the-loop experimental results, we examine human drivers' reactions in complex driving scenarios and demonstrate the effectiveness of the developed method.**

***Index Terms*—Cooperative driving, connected vehicles, autonomous vehicles, stochastic model predictive control, hybrid system, mixed integer programming.**

I. Introduction

AUTONOMOUS vehicles (AVs) are increasingly making their way into the transportation systems. AVs are already a reality due to advances in sensors, computers, and machine learning algorithms. In terms of safety, efficacy, and accessibility, AVs have the potential to enhance transportation efficiency for people all over the world. According to [1], more than 33 million AVs will be sold worldwide by 2040, with 7.4 million sold in the United States, 14.5 million in China, 5.5 million in European nations, and 6.3 million in other foreign markets. AVs and human-driven cars are anticipated to coexist for a long time in the future. As a result, it is critical to explore how to ensure safety in mixed traffic that includes both AVs and human-driven cars. Cooperative driving between AVs and human-driven vehicles can be an effective method to increase transportation safety and efficiency.

[1]Sanzida Hossain and He Bai are with Mechanical and Aerospace Engineering, Oklahoma State University, Stillwater, OK 74078, USA. {sanzida.hossain, he.bai}@okstate.edu

[2]Jiaxing Lu and Weihua Sheng are with Electrical and Computer Engineering, Oklahoma State University, Stillwater, OK 74078, USA. {jiaxing.lu,weihua.sheng}@okstate.edu

A. Problem Statement

In this paper, we examine cooperative driving between AVs and human-driven vehicles in a connected environment. We envision a human-driven vehicle that can communicate with other vehicles and offer guidance to its driver. Such a vehicle is referred to as an intelligent human-driven vehicle (IHV). An IHV features an integrated copilot that monitors the states of the human driver and issues advising directives to affect the human driver's actions. It can also sense its surroundings and exchange information with nearby connected vehicles via vehicle-to-vehicle (v2v) communication. We also consider unconnected and uncontrollable vehicles in the surroundings, which are called obstacle vehicles (OBS).

The IHV dynamics is a sophisticated hybrid system dependent on the human driver's condition and actions. Human states must be properly assessed for optimal coordination between an IHV and AVs. Furthermore, the predicted human behavior must be communicated between the coordinating vehicles before being included into an optimal decision-making problem. In this paper, we introduce a framework for assessing and applying human state information into cooperative driving to influence the behavior of the human driver in the IHV and design the control inputs for the AVs.

B. Contributions

Modeling an IHV is a difficult subject since it is dependent on the human driving style. We suggest modeling the IHV as a discrete system that shifts between distinct dynamics dependent on the condition of the human driver. To generate control inputs and advisory commands for the AVs and the IHV, we employ discrete hybrid stochastic automata (DHSA) [2] as a tool to formulate their interactions and develop a stochastic model predictive control (sMPC) approach. In [3]–[5], we outline the optimization of cooperative driving between an IHV and an AV. In [6] we explore a three-vehicle merging scenario and assess the performance with simulations and experiments. In these prior efforts, we consider a fixed number of vehicles and a specific lane merging scenario and focus on the longitudinal states of the vehicles. Thus, only the longitudinal control commands are designed to achieve a safe gap for merging. While our previous work is effective in creating gaps for merging, it lacks generality with respect to the number of vehicles involved and does not consider lateral advising, such as lane change.

Building on [3]–[6], in this paper we construct a multi-vehicle, multi-lane lane-changing cooperative driving framework to accommodate more complex driving scenarios and an arbitrary number of vehicles. The generation of safe and efficient lane-changing and merging behaviors becomes more complicated to model than in the previous work. We introduce discrete lane states to indicate vehicles on different lanes, and develop logical conditions consisting of both lane states and longitudinal states to achieve coordination. Behaviors of vehicles in adjacent lanes are considered and predicted to produce both longitudinal and lateral control inputs for the AVs and advisory commands for the IHVs. We also consider surrounding unconnected and uncontrollable vehicles, making the formulation applicable to more realistic road scenarios.

In this formulation, we model the human driver with two stochastic human states: the driver's attentiveness and the probability of following advisory commands. These stochastic states are estimated online using machine learning techniques. We employ a residual network (ResNet-50) to detect distracted driving behaviors by recognizing various characteristics in video frames to evaluate the probability of human attentiveness. We use a Hidden Markov Model (HMM)-based probability model to recognize the human driver's behaviors and then compare them to previously recommended advisory to estimate the driver's tendency to follow advisory commands.

We conduct a sensitivity analysis to assess the performance of our approach with respect to varying errors in the transition probabilities of the human states. The sensitivity analysis demonstrates robustness of our method against such errors. To evaluate the effectiveness of our formulation, we design and conduct simulations and human-in-the-loop (HITL) experiments in an emergency driving scenario. The HITL experiments demonstrate that our method enhances safety by reducing the number of collision events in a complex emergency driving scenario.

The main contributions of the paper are summarized below.

1) We develop a cooperative driving framework to address multi-lane, multi-vehicle scenarios with a multi-state human driver model, which significantly improves our previous work [3]–[6]. This framework also considers unconnected and uncontrollable obstacle vehicles. The framework provides optimal longitudinal and lane change inputs and advising commands to coordinate the AVs and the IHVs, making it capable of addressing complex vehicle coordination problems.
2) We conduct a sensitivity analysis to reveal the impact of parameter errors on the system performance.
3) We perform HITL experiments in a complex emergency-stopping scenario and demonstrate the effectiveness of our formulation.

The rest of this paper is organized as follows. We discuss related work in Section II. A review of the DHSA method is presented in Section III. The vehicle dynamic models are described in Section IV. The formulation of vehicle coordination is developed in Section V. In Section VI, we present the sMPC for vehicle coordination. We assess the feasibility of our formulation through simulation results in Section VII and evaluate the effectiveness using HITL experiments in Section VIII. Section IX presents the concluding remarks and future work.

II. Related work

In this section, we discuss recent research in the field of autonomous vehicles to accommodate human-driven vehicles in mixed traffic.

A. Human driver modeling for autonomous vehicles

Appropriate modeling of stochastic components in human actions is critical to facilitate cooperative driving. In the past decade, researchers have worked on human driver modeling for applications in driving assistance systems. In [7], the authors model the interaction between the driver and the vehicle in an assistance driving system using hidden mode stochastic hybrid systems. Furthermore, by tracking both human behavior and vehicle state, they improve decision-making and infer the human condition. Partially observable Markov decision processes (POMDPs) are utilized in [8] to establish a unified framework describing machine dynamics and human behavior in HITL control of semi-autonomous vehicles. The authors of [9] simulate the human driver's lateral tracking reaction while taking physical limits and numerous driver variables into account. These characteristics distinguish human drivers and serve to identify human control behavior for vehicle control. A human driver path following model is explored in [10] as a blend of perception, decision, and execution models. Reference [11] offers a driver model based on human subject driving simulator experiments for both lateral and longitudinal motions. They can identify distinct driving behaviors for the human driver model by identifying driver model parameters. The authors of [12] introduce a model for human speed prediction combining a first-principle approach with a Gaussian process (GP) machine learning model and implement it in a chance-constrained MPC strategy for AV, which enhances vehicle safety and efficiency in mixed traffic and outperforms traditional MPC methods. The driver's mental state, the context or circumstance in which the vehicle is in, and the surrounding environment are analyzed in [13] to forecast human driving behavior over long time horizons. In [14] the authors use transfer learning in conjunction with a convolutional neural network to generate a model for driving behavior recognition where the sample size is relatively small.

Although [7], [8] model a human driver as a hybrid system and consider stochasticity of human drivers, they are applicable only to a single vehicle and do not consider applications in connected vehicles. References [9]–[12] explore different approaches of human driver modeling for specific driving tasks, such as longitudinal and lateral tracking. References [13], [14] develop different methods for human driver modeling based on discrete human states. In this paper, we also make use of discrete human states to model human-driven vehicles.

B. Human driver and AV interaction

The design of an autonomous vehicle is a challenging task. With human-driven vehicles co-existing in the environment, the problem becomes more complex. When the system is unpredictable owing to human interaction or road circumstances, [15] formulates risk-bounded mobility strategies for

AVs using a chance-constrained POMDP. In [16] the authors consider modeling the interaction of a human-driven vehicle with an AV in a game theoretic interaction model. The authors determine how closely a human follows the game-theoretic interaction model by defining the influence between the human and the robot as unobserved latent variables. The authors of [17] develop a lane-changing decision model for autonomous vehicles (AVs) that accounts for surrounding vehicles and trajectory planning using a multi-player dynamic game model to enhance safety and efficiency in mixed traffic scenarios. Reference [18] explores the evolving characteristics of trust levels of human drivers on AVs and their impact on driving behaviors. In [19], the authors explore the effect of aggressive driving by human drivers on AVs in a mixed traffic flow. The question that how AVs impact the behavior of human-driven cars is investigated in [20]. They employ planned interactions to affect human behavior to save fuel consumption and trip time. Reference [21] examines how the existence of AVs in mixed traffic influences the car following model of human drivers.

In summary, [15]–[17] model the stochastic human-AV interaction and develop decision models of AVs in different scenarios. However, the human-driven vehicles are not actively involved in the coordination. References [18], [19] explore effects of human drivers and their driving behaviors on AVs while [20], [21] explore the impact of AVs on human driver behaviors. Coordination of these two types of vehicles is not considered.

Fuzzy control has been utilized to address autonomous vehicle decision-making in mixed traffic scenarios. Reference [22] develops and tests a system that detects an approaching vehicle at an intersection and uses fuzzy logic to design the maneuver of the AV at the intersection. In [23], the authors explore risk-aware fuzzy control of AV enabling it to identify potential collision, assess its level of risk, and reduce the associated risks by speed reduction or stopping the AV if necessary. Reference [24] introduces a fuzzy control approach to design automated longitudinal vehicle control for adaptive cruise controllers. In [25], the authors present the effect of uncertainty on the driver lane change model and develop a novel lane change model incorporating dynamic vehicle characteristics and fuzzy factors. Fuzzy controls are typically applied to unknown system dynamics and modify the outputs based on a rule set. In this paper, the vehicles are connected and their dynamic models are assumed known. MPC controllers work well in this case where the system dynamics are available.

C. *Connected autonomous vehicles in mixed traffic*

As AV technology moves towards a connected environment, recent research focus has mostly been on designing coordination between connected AVs (CAVs). The authors of [26] use multi-agent reinforcement learning to model CAV lane-changing decision-making in a mixed-traffic highway situation. In [27], the authors create a ramp inflow coordination and merging control model for hybrid automatic driving. Their methodology uses game theory to optimize both safety and efficiency under various scenarios in order to discover the best strategy. Reference [28] examines the control of linked AVs to respond appropriately to unpredictable human-driven vehicle motions. Reference [29] proposes a control strategy for a freeway merging scenario with a dedicated CAV lane and a human-driven vehicle lane, aiming to enhance fuel economy and improve traffic efficiency. The trajectories of CAVs are optimized to allow seamless merging into available gaps in traffic. Reference [30] finds that optimal AV foresight, vehicle density, and AV-to-HV ratio are key to maximizing traffic flow and avoiding congestion in a mixed traffic scenario. Reference [31] uses a cellular automaton model and finds that CAVs improve traffic parameters such as velocity, flow, and critical density, reducing congestion significantly compared to human-driven vehicles. Reference [32] explores a controller role for CAVs by synchronizing the speed and alignment of CAVs and acting as platoon leaders to guide the human drivers and regulate mixed traffic at intersections.

To summarize, [26]–[29] have focused on modeling coordination between CAVs in a mixed traffic scenario considering human drivers' stochasticity. References [30], [31] examine the effect of CAVs on the traffic flow.

Existing literature has mainly focused on human-AV interaction, human-driver reaction modeling, and the effects of human drivers in CAV coordination in mixed traffic. In these studies, human-driven vehicles are considered unconnected and uncontrollable entities and the AVs are designed to adapt to surrounding human-driven vehicles but without actively involving the human-driven vehicles in cooperative driving. In [20], [32], human drivers are influenced by AV maneuvers to regulate the traffic flow. Our work, on the contrary, is focused on human-AV cooperative driving in a connected environment where a human driver is actively influenced by advisory commands. To the best of our knowledge, we are the first to explore and develop solutions to this challenging cooperative driving problem.

III. Review of DHSA

A hybrid system contains both continuous and discrete states and inputs. Modeling such a system with stochasticity is challenging. Introduced in [2], DHSA is a popular mathematical tool to formulate discrete hybrid stochastic systems. In [33], [34], DHSA is used to model the hybrid nature of a vehicle system. In our problem, there are continuous vehicle states such as its position and velocity, and discrete states such as vehicle's lane, human driver's attentiveness, and tendency to follow advisory. Due to the hybrid nature of the combined driver-vehicle system, we choose to employ DHSA to model the vehicle dynamics. In this section, we present a brief review of DHSA from [2].

A DHSA consists of four components: a switched affine system (SAS), an event generator (EG), a mode selector (MS), and a stochastic finite state machine (sFSM). The system's propagation model is defined with the SAS

$$x_{c_{k+1}} = A_{i_k} x_{c_k} + B_{i_k} u_{c_k} + f_{i_k} \tag{1}$$

where $k \in \mathbb{Z}_{0+}$ is the discrete time index of the system. The continuous states are denoted by $x_{c_k} \in \mathbb{R}^{n_c}$, where n_c

is the number of continuous states. The continuous inputs are denoted by $u_{c_k} \in \mathbb{R}^{m_c}$, where m_c is the number of continuous inputs to the system. The system switches between different modes defined by $i_k \in I \triangleq \{1, 2, \cdots, s\}$. Based on the current mode of the system i_k the dynamics is defined with $\{A_i, B_i, f_i\}_{i \in I}$, which are constant matrices of suitable dimensions.

The EG produces binary event signals δ_{e_k} based on the continuous states and inputs, defined as

$$\delta_{e_k} = f_{EG}(x_{c_k}, u_{c_k}) \tag{2}$$

where $\delta_{e_k} \in \{0,1\}^{n_e}$ and n_e is the number of generated binary event signals. The event generation function $f_{EG} : \mathbb{R}^{n_c+m_c} \rightarrow \{0,1\}^{n_e}$ is given by

$$[f^j_{EG}(x_c, u_c) = 1] \leftrightarrow [H^j_e x_c + J^j_e u_c + K^j_e \leq 0] \tag{3}$$

in which $H_e \in \mathbb{R}^{n_e \times n_c}$, $J_e \in \mathbb{R}^{n_e \times m_c}$, and $K_e \in \mathbb{R}^{n_e}$ are constant matrices defining linear threshold conditions. The superscript j denotes the j^{th} row. The EG function triggers an event based on the continuous states and inputs.

The MS is defined by a Boolean function $f_{MS} : \{0,1\}^{n_b+m_b+n_e} \rightarrow I$ where n_b is the number of binary states and m_b is the number of binary inputs. It takes the binary states, binary inputs and binary event signals as inputs and selects the mode i_k for (1). It can be defined as

$$i_k = f_{MS}(x_{b_k}, u_{b_k}, \delta_{e_k}) \tag{4}$$

where $x_b \in \{0,1\}^{n_b}$ is the vector of binary states and $u_b \in \{0,1\}^{m_b}$ is the vector of binary inputs.

The sFSM is a Boolean function $f_{sFSM} : \{0,1\}^{2n_b+m_b+n_e} \rightarrow [0,1]$ satisfying

$$p[x_{b_{k+1}} = \hat{x}_b] = f_{sFSM}(x_{b_k}, u_{b_k}, \delta_{e_k}, \hat{x}_b) \tag{5}$$

where $p[\cdot]$ denotes the probability of a transition. The state machine measures the probability of the next discrete state taking a certain value based on the current binary states, binary inputs, binary event signals, and the current discrete state.

An illustration of DHSA is shown in Fig. 1.

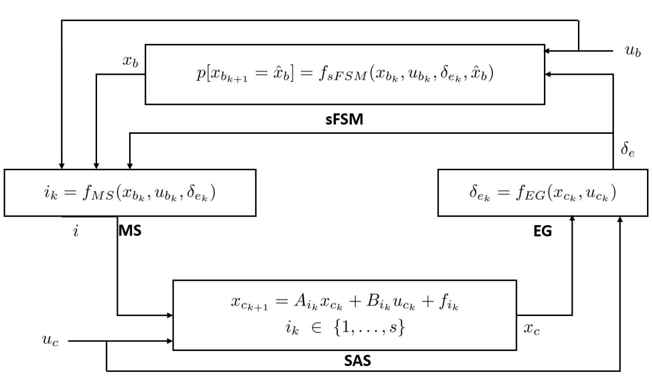

Fig. 1. Discrete hybrid stochastic automata (DHSA) [2].

IV. Vehicle dynamics

A. Vehicle dynamics of IHV

We model the IHV dynamics as a DHSA reviewed in Section III. The states of the human driver are considered discrete states. Based on the discrete states, the IHV dynamics switch between several models. The IHV dynamics are defined in the same manner as the SAS in the DHSA. We use the sFSM and MS of the DHSA to model the human state transition events in the IHV.

The set of potential human states is denoted by one hot encoded vector $S_k = [s^1_k, s^2_k, \ldots, s^n_k]^\top \in \mathbb{Z}^n$ where $s^1_k, s^2_k, \ldots, s^n_k \in \{0,1\}$ represent discrete human states and n is the total number of possible states. Only one element in S_k is 1, while the rest are zeros. Each non-zero s^i_k, where $i \in \{1, \cdots, n\}$, represents a specific combination of behavioral aspects of the human driver being considered.

Let the binary variable $u^B_k \in \{0,1\}$ define the advisory status of the IHV for the time step k. If the advisory is on then $u^B_k = 1$, otherwise $u^B_k = 0$. We focus on two characteristics of human driver behavior in particular: the human driver's advisory following state denoted by $x^B_k \in \{0,1\}$ and the attentiveness state denoted by $a_k \in \{0,1\}$. The human driver's advisory following state $x^B_k = 1$ indicates that the driver is following the advisory and $x^B_k = 0$ indicates that the human driver is not following the advisory and rather driving on his/her own will. The attentiveness state $a_k = 1$ when the human driver is attentive and $a_k = 0$ otherwise. Considering x^B_k and a_k, there can be four human states in total :

1) distracted $(a_k = 0)$ and not following $(x^B_k = 0)$
2) distracted $(a_k = 0)$ and following $(x^B_k = 1)$
3) attentive $(a_k = 1)$ and not following $(x^B_k = 0)$
4) attentive $(a_k = 1)$ and following $(x^B_k = 1)$

Human drivers tend to behave similarly while distracted, regardless of whether they follow directions or not. As a result, we combine the four states into $S_k = [s^1_k, s^2_k, s^3_k]$ defined as

$$s^1_k = 1 \Leftrightarrow (a_k = 0) \wedge (x^B_k = 0 \vee 1), \tag{6}$$
$$s^2_k = 1 \Leftrightarrow (a_k = 1) \wedge (x^B_k = 0), \tag{7}$$
$$s^3_k = 1 \Leftrightarrow (a_k = 1) \wedge (x^B_k = 1). \tag{8}$$

In (6), the 'distracted following' state and the 'distracted not following' state are considered the same state. Depending on the current human state, the dynamics of the IHV is given by

$$s^1_k = 1 \Rightarrow x^h_{k+1} = A_h x^h_k + B_h u^d_k, \tag{9}$$
$$y^a_{k+1} = u^d_k, \tag{10}$$
$$s^2_k = 1 \Rightarrow x^h_{k+1} = A_h x^h_k + B_h u^h_k, \tag{11}$$
$$y^a_{k+1} = u^h_k, \tag{12}$$
$$s^3_k = 1 \Rightarrow x^h_{k+1} = A_h x^h_k + B_h y^a_k, \tag{13}$$
$$y^a_{k+1} = \lambda y^a_k + (1 - \lambda) u^a_k, \tag{14}$$

where the longitudinal position and velocity with respect to the origin are represented by $x^h_k \in \mathbb{R}^2$ and A_h and B_h are matrices of suitable dimensions that define the IHV dynamics, the state y^a_k holds the input applied from the previous step to account for the delay, $u^d_k \in \mathbb{R}$ is the human input when the human is distracted, $u^h_k \in \mathbb{R}$ is the human input when the human is not distracted (attentive), and $u_k^a \in \mathbb{R}$ is the advisory commands for the IHV. The lateral lane state of the vehicles is discussed with the lane advisory constraints in subsection IV-A2.

The human inputs can be estimated using different methods. One approach is to employ an HMM-based probabilistic transition model to predict the human driver's future actions, as presented in [6]. For this paper, we predict the human inputs u_k^d and u_k^h as a trajectory using the method presented in [4].

In (13) and (14) where $s_k^3 = 1$, the human attempts to obey a provided advisory control. There is a delay when the human driver attempts to implement an advisory directive. As a result, rather than being applied to the vehicle immediately, the advising command is carried out gradually by the human driver. More delays may occur as a result of computational, transmission, and notification delays of the advised commands. To account for these delay effects, we employ a first-order system of the form (14). When we set the longitudinal reaction constant λ in (14) to 0, the driver applies the advised control command u_k^a exactly at the $(k+1)^{th}$ step, i.e., with one step delay. It is anticipated that the calculation, announcement, and driver tracking of the advisory directives is completed in this one step delay. As λ increases to 1, the driver's response to the advisory action u_k^a is further slowed down. Thus, $\lambda \in [0,1)$ represents how fast the human in the IHV is adapting to the advisory action u_k^a after it is announced. We can modify (14) to accommodate longer delays. The first-order delay model can be replaced by other human actuation dynamics, such as the second-order dynamics in [9], [35].

Define $\bar{x}_k^h = [x_k^h; y_k^a]$. We rewrite the dynamics (9)–(14) as

$$\bar{x}_{k+1}^h = \begin{pmatrix} A_h & 0 \\ 0 & 0 \end{pmatrix} \bar{x}_k^h + \begin{pmatrix} B_h & B_h & B_h & 0 \\ 1 & \lambda & 1 & (1-\lambda) \end{pmatrix} \begin{pmatrix} s_k^1 u_k^d \\ s_k^3 y_k^a \\ s_k^2 u_k^h \\ s_k^3 u_k^a \end{pmatrix}$$

$$= \begin{pmatrix} A_h & 0 \\ 0 & 0 \end{pmatrix} \bar{x}_k^h + \begin{pmatrix} B_h & B_h & B_h & 0 \\ 1 & \lambda & 1 & (1-\lambda) \end{pmatrix} \begin{pmatrix} \bar{z}_k^1 \\ \bar{z}_k^2 \\ \bar{z}_k^3 \\ \bar{z}_k^4 \end{pmatrix}, \quad (15)$$

where $\bar{z}_k^1 = s_k^1 u_k^d$, $\bar{z}_k^2 = s_k^3 y_k^a$, $\bar{z}_k^3 = s_k^2 u_k^h$, and $\bar{z}_k^4 = s_k^3 u_k^a$. Based on $\bar{z}_k^1$, $\bar{z}_k^2$, $\bar{z}_k^3$, $\bar{z}_k^4$, and the initial conditions x_0^h, we obtain the solution to x_k^h and y_k^a as:

$$x_k^h = A_h^k x_0^h + \sum_{j=0}^{k-1} A_h^{k-j-1} B_h \bar{z}_j^1 + \sum_{j=0}^{k-1} A_h^{k-j-1} B_h \bar{z}_j^2 + \sum_{j=0}^{k-1} A_h^{k-j-1} B_h \bar{z}_j^3, \quad (16)$$

$$y_k^a = \bar{z}_{k-1}^1 + \lambda \bar{z}_{k-1}^2 + \bar{z}_{k-1}^3 + (1-\lambda)\bar{z}_{k-1}^4. \quad (17)$$

The IHV dynamics are subject to constraints that are categorized into four categories: 1) state constraints, 2) lane advisory constraints, 3) human state transition constraints, and 4) chance constraints.

1) State constraints: The new variables $\bar{z}_k^1, \bar{z}_k^2, \bar{z}_k^3$ and $\bar{z}_k^4$ and their relationships with the states and inputs lead to state constraints. The state and input limits are also included in these constraints. These constraints are formulated as

$$\bar{z}_k^1 \le M_u s_k^1, \ \bar{z}_k^1 \ge m_u s_k^1, \quad (18)$$

$$\bar{z}_k^1 \le u_k^d - m_u(1-s_k^1), \ z_k^1 \ge u_k^d - M_u(1-s_k^1), \quad (19)$$

$$\bar{z}_k^2 \le M_u s_k^3, \ \bar{z}_k^2 \ge m_u s_k^3, \quad (20)$$

$$\bar{z}_k^2 \le y_k^a - m_u(1-s_k^3), \ \bar{z}_k^2 \ge y_k^a - M_u(1-s_k^3), \quad (21)$$

$$\bar{z}_k^3 \le M_u s_k^2, \ \bar{z}_k^3 \ge m_u s_k^2, \quad (22)$$

$$\bar{z}_k^3 \le u_k^h - m_u(1-s_k^2), \ \bar{z}_k^3 \ge u_k^h - M_u(1-s_k^2) \quad (23)$$

$$\bar{z}_k^4 \le M_u s_k^3, \ \bar{z}_k^4 \ge m_u s_k^3, \quad (24)$$

$$\bar{z}_k^4 \le u_k^a - m_u(1-s_k^3), \ \bar{z}_k^4 \ge u_k^a - M_u(1-s_k^3). \quad (25)$$

Here the upper and lower bounds of the input acceleration are denoted by M_u and m_u respectively.

Any state limits of the IHV can be enforced by the following constraints:

$$x_k^h \le M, \ \ x_k^h \ge m, \quad (26)$$

for some upper limit M and lower limit m.

2) Lane advisory constraints: To model the lateral state and control of the vehicles, we introduce a discrete lane state for each vehicle. Let $L_k^v \in \mathbb{Z}_+$ be a discrete variable denoting the lane index for vehicle v. Let n_l be the total number of lanes in the road. Then $L_k^v \in \{1, 2, \cdots, n_l\}$. For example, $L_k^v = 1$ and $L_k^v = n_l$ mean that vehicle v is on the leftmost and rightmost lane, respectively.

When a vehicle performs a lane change to an adjacent lane, it may take a number of time steps to complete, i.e., the lane change is not instantaneous. Suppose that it takes $f^v \in \mathbb{Z}_+$ discrete time steps to complete the lane change. Let $F_k^v = \{k - f^v + 1, k - f^v + 2, \cdots, k\}$. We introduce $a_k^v \in \{1, 2, \cdots, n_l\}$ as the advised lane index for vehicle v at time step k and design the following constraints to accommodate non-instantaneous lane changes:

$$a_q^v - L_{k+1}^v \le \bar{M}(1 + (L_k^v - L_{k+1}^v)) \ \forall q \in F_k^v, \quad (27)$$

$$a_q^v - L_{k+1}^v \ge -\bar{M}(1 + (L_k^v - L_{k+1}^v)) \ \forall q \in F_k^v, \quad (28)$$

$$a_q^v - L_{k+1}^v \le \bar{M}(1 - (L_k^v - L_{k+1}^v)) \ \forall q \in F_k^v, \quad (29)$$

$$a_q^v - L_{k+1}^v \ge -\bar{M}(1 - (L_k^v - L_{k+1}^v)) \ \forall q \in F_k^v. \quad (30)$$

From these constraints, we see that for a lane change to complete at the $(k+1)$th step, i.e., $L_k^v - L_{k+1}^v = \pm 1$, the condition $a_q^v = L_{k+1}^v$, $\forall q \in F_k^v$, must be satisfied. That is, before completing the lane change, the vehicle must be advised for f^v steps to switch to lane L_{k+1}^v. During these f^v steps, the vehicle transitions from lane L_k^v to L_{k+1}^v.

3) Human state transition constraints: We consider human state transitions from s_k^i to s_{k+1}^j as stochastic events. To model these transitions, we define one hot encoded variable $t_k = [t_k^1, t_k^2, \ldots, t_k^{n^2}]$, where n is the number of discrete human states. Here, each element $t_k^p \in \{0,1\}, \ \forall \ p \in \{1, 2, \ldots, n^2\}$, indicates an event of transitioning from $s_k^i = 1 \rightarrow \ s_{k+1}^j = 1$ when $u_k^B = 1$ (advising on) where $i, j \in \{1, 2, \ldots, n\}$. Similarly, we define one hot encoded $\bar{t}_k = [\bar{t}_k^1, \bar{t}_k^2, \ldots, \bar{t}_k^{n^2}]$, where each element $\bar{t}_k^p \in \{0,1\}, \ \forall \ p \in \{1, 2, \ldots, n^2\}$, indicates an event of

This article has been accepted for publication in IEEE Transactions on Vehicular Technology. This is the author's version which has not been fully edited and content may change prior to final publication. Citation information: DOI 10.1109/TVT.2025.3584022

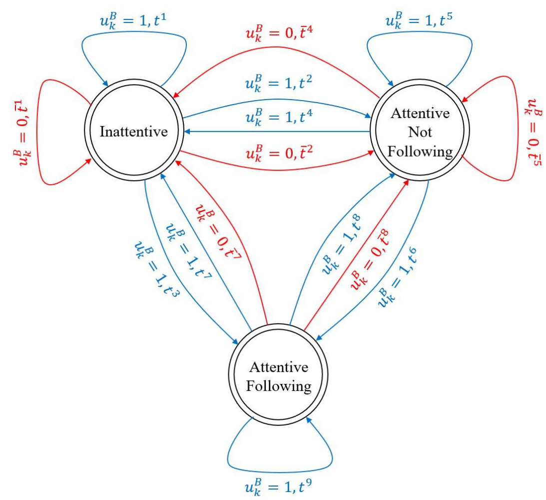

Fig. 2. Stochastic finite state machine for human state transitions. The blue transitions indicate the transitions for $u_k^B = 1$ and the red transitions indicate the transitions for $u_k^B = 0$.

transitioning from $s_k^i = 1 \rightarrow s_{k+1}^j = 1$ when $u_k^B = 0$ (advising off) where $i, j \in \{1, 2, \ldots, n\}$.

The transitions in our system where $n = 3$ are illustrated as an sFSM in Fig. 2. The total number of possible transitions is 18. Among these transitions, the transitions that are not possible to occur have probabilities of 0, which are not shown in the sFSM. In total, there are 15 transitions.

Following the human state transition from the sFSM, each transition from s_k^i to s_{k+1}^j for $u_k^B = 1$ is encoded by the binary event t_k^p. Therefore, the event t_k^p takes place only when $s_k^i = s_{k+1}^j = u_k^B = 1$. This is similar to the MS function in the DHSA. These transitions are converted to the following inequality constraints:

$$s_{k+1}^j + s_k^i + u_k^B \leq 2 + t_k^p, \tag{31}$$

$$t_k^p \leq s_k^i, \tag{32}$$

$$t_k^p \leq s_{k+1}^j, \tag{33}$$

$$t_k^p \leq u_k^B. \tag{34}$$

Similarly, each transition from s_k^i to s_{k+1}^j when $u_k^B = 0$ is encoded by the binary event $\bar{t}_k^p$ and the event $\bar{t}_k^p$ takes place only when $s_k^i = s_{k+1}^j = (1 - u_k^B) = 1$. This transition is formulated using the following inequalities:

$$s_{k+1}^j + s_k^i - u_k^B \leq 1 + \bar{t}_k^p, \tag{35}$$

$$\bar{t}_k^p \leq s_k^i, \tag{36}$$

$$\bar{t}_k^p \leq s_{k+1}^j, \tag{37}$$

$$\bar{t}_k^p \leq (1 - u_k^B). \tag{38}$$

Each event pair $\{t_k^p, \bar{t}_k^p\}$, $\forall p \in \{1, 2, \ldots, 3^2\}$ produces constraints similar to (31)–(38). Since only one event occurs in the k^{th} time step, it follows that

$$t_k^1 + t_k^2 + \cdots + t_k^{n^2} + \bar{t}_k^1 + \bar{t}_k^2 + \cdots + \bar{t}_k^{n^2} = 1. \tag{39}$$

The transition probability of an event t_k^p is denoted by $P(t_k^p) = P(s_{k+1}^j = 1 | s_k^i = 1, u_k^B = 1)$. Similarly the transition probability of an event $\bar{t}_k^p$ is denoted by $P(\bar{t}_k^p) = P(s_{k+1}^j = 1 | s_k^i = 1, u_k^B = 0)$. These transition probabilities indicate the human's driving pattern and level of compliance, which can be estimated based on prior driving data. For simulation and experimental demonstrations, we have chosen the transition probabilities given in Appendix A.

4) Chance constraints: Chance constraints are used to eliminate from the set of potential solutions any trajectories that only happen with a small probability. The potential human state transition events in our formulation are $T_k = \begin{bmatrix} t_k^1 & \ldots & t_k^{n^2} & \bar{t}_k^1 & \ldots & \bar{t}_k^{n^2} \end{bmatrix}^\top$ and the transition probabilities are $P = \begin{bmatrix} P[t_k^1] & \ldots & P[t_k^{n^2}] & P[\bar{t}_k^1] & \ldots & P[\bar{t}_k^{n^2}] \end{bmatrix}^\top$. Following [2], the probability of the state trajectory is

$$\begin{bmatrix} \pi_0 \\ \vdots \\ \pi_{K-1} \end{bmatrix} = \begin{bmatrix} T_0^\top \\ \vdots \\ T_{K-1}^\top \end{bmatrix} P, \tag{40}$$

where K is the look-ahead window in the MPC. Here, π_k is the dot product of the potential human state transitions T_k with probabilities of those transitions. At step k, π_k indicates the likelihood of taking the transition described by T_k. The probability of the whole T trajectory, $\pi(T)$, is given by

$$\pi(T) = \pi(T_0, T_1, \ldots, T_k) = \prod_{k=0}^{K-1} \pi_k. \tag{41}$$

Then the chance constraint is formulated as

$$\pi(T) \geq \tilde{p}, \tag{42}$$

with $\tilde{p} \in [0, 1]$ being a probability bound. This chance constraint (42) enforces that T realizes with at least $\tilde{p}$ probability.

For a look ahead window of K, the decision variables for each IHV are summarized as $\alpha_k^i = [\mathbf{u}_k^a \; \bar{\mathbf{z}}_k^1 \; \bar{\mathbf{z}}_k^2 \; \bar{\mathbf{z}}_k^3 \; \bar{\mathbf{z}}_k^4 \; \mathbf{u}_k^B \; \mathbf{L}_k \; \mathbf{a}_k \; \mathbf{s}_k^1 \; \mathbf{s}_k^2 \; \mathbf{s}_k^3 \; \mathbf{t}_k^1 \; \mathbf{t}_k^2 \; \ldots \; \mathbf{t}_k^{3^2} \; \bar{\mathbf{t}}_k^1 \; \bar{\mathbf{t}}_k^2 \; \ldots \; \bar{\mathbf{t}}_k^{3^2}]$ where $i \in \{1, 2, \ldots, n^h\}$ is the IHV index for total number of IHVs being n^h. $\mathbf{u}_k^a = \begin{bmatrix} u_k^a, & u_{k+1}^a, & \cdots, & u_{k+K-1}^a \end{bmatrix}$ and all the other decision variables are defined similarly. The continuous variables are $\mathbf{u}_k^a$, $\bar{\mathbf{z}}_k^1$, $\bar{\mathbf{z}}_k^2$, $\bar{\mathbf{z}}_k^3$, *and* $\bar{\mathbf{z}}_k^4$ while the rest are binary.

B. Vehicle dynamics of AV

We consider a linear dynamic model of an AV

$$x_{k+1}^r = A_r x_k^r + B_r u_k^r, \tag{43}$$

where the longitudinal position and velocity with respect to the origin are represented by $x_k^r \in \mathbb{R}^2$, A_r and B_r are matrices of suitable dimensions that define the AV dynamics, and $u^r \in \mathbb{R}$ is the input (acceleration) to the AV. Based on the initial conditions x_0^r, we obtain the solution to x_k^r as

$$x_k^r = A_r^k x_0^r + \sum_{j=0}^{k-1} A_r^{k-j-1} B_r u_j^r. \tag{44}$$

The AV is a comparatively simple system that is directly controlled by the control inputs. Unlike the IHVs the AVs only have state limit constraints and lane advisory constraints.

The state limit constraints enforce respective state limits for each AV:

$$x_k^r \leq M, \quad x_k^r \geq m \tag{45}$$

for some upper limit M and lower limit m.

Similar to the IHV, each AV has the discrete lane state $L_k^v \in \{1, 2 \ldots, n_l\}$ for vehicle v and the advising lane index $a_k^v \in \{1, 2 \ldots, n_l\}$. Each AV has similar lane advisory constraints to (27)–(30).

For a look ahead window of K, the independent decision variables for AV are $\beta_k^j = [\mathbf{u}_k^r \ \mathbf{L}_k \ \mathbf{a}_k]$ where $j \in \{1, 2, \ldots, n^r\}$ is the AV index for total number of AVs being n^r and $\mathbf{u}_k^r = \begin{bmatrix} u_k^r, & u_{k+1}^r, & \cdots, & u_{k+K-1}^r \end{bmatrix}$ and all other decision variables are defined similarly.

C. Dynamics of OBS

The OBS is an unconnected and uncontrollable vehicle. We assume that the current position and velocity of the OBS are available. We consider a similar dynamic model of the OBS to the AVs:

$$x_{k+1}^o = A_o x_k^o + B_o u_k^o, \tag{46}$$

where the longitudinal position and velocity with respect to the origin are represented by $x_k^o \in \mathbb{R}^2$, A_o and B_o are matrices of suitable dimensions that define the OBS dynamics, and $u^o \in \mathbb{R}$ is the input (acceleration) to the OBS.

V. Vehicle coordination

We address the coordination of AVs and IHVs in a driving scenario illustrated in Fig. 3. The number of IHVs is n^h and the number of AVs is n^r. We consider an OBS in the scenario that suddenly stops in its lane. The main objective of all the connected vehicles is to safely maneuver around the OBS. Here, the AVs can be directly controlled via control inputs. Advisory instructions can influence the driver's actions which change the IHV's motion. The OBS is uncontrollable and the connected vehicles have the position and velocity information of the OBS.

We next present state and control constraints between adjacent vehicles and develop the coordination algorithm to find optimal advisory instructions and autonomous controls for the IHV and the AVs, respectively.

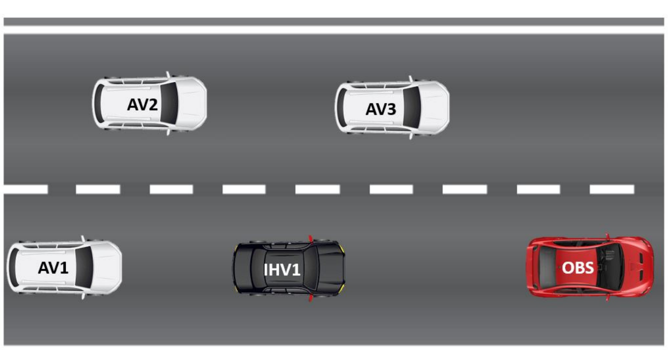

Fig. 3. A five-vehicle coordination scenario with 1 IHV, 3 AVs, and 1 OBS.

A. Coordinating constraints

To model the lateral coordination between vehicles, we consider the relative lane position between any two vehicles, say v1 and v2. Define a two-dimensional integer vector $l_k^{v1v2} \in \{0, 1\}^{2\times 1}$ to indicate the relative lane states between v1 and v2. If they are in the same lane, $l_k^{v1v2} = [1 \ 0]^\top$. If they are in adjacent lanes, $l_k^{v1v2} = [0 \ 1]^\top$. Otherwise $l_k^{v1v2} = [0 \ 0]^\top$. For the same-lane vehicles, the constraint $l_k^{v1v2} = [1 \ 0]^\top$ can be enforced by the following inequalities

$$L_k^{v1} - L_k^{v2} \leq 0 + \bar{M}(1 - l_{1,k}^{v1v2}), \tag{47}$$

$$L_k^{v1} - L_k^{v2} \geq 0 - \bar{M}(1 - l_{1,k}^{v1v2}), \tag{48}$$

$$l_{1,k}^{v1v2} + l_{2,k}^{v1v2} \leq 1, \tag{49}$$

where $l_{1,k}^{v1v2}$ and $l_{2,k}^{v1v2}$ are the 1st and 2nd element of l_k^{v1v2}, respectively, and $\bar{M}$ is sufficiently large. These two constraints ensure that when $v1$ and $v2$ are in the same lane meaning $L_k^{v1} - L_k^{v2} = 0$, the value of $l_{1,k}^{v1v2}$ is 1.

For vehicles in adjacent lanes, there are two possibilities: $L_k^{v1} - L_k^{v2} = 1$ or $L_k^{v1} - L_k^{v2} = -1$. For this discontinuity, we introduce another two-dimensional binary vector $\alpha_k^{v1v2} \in \{0, 1\}^{2\times 1}$ and define the following inequalities

$$L_k^{v1} - L_k^{v2} \geq \varepsilon - \bar{M}(1 - \alpha_{1,k}^{v1v2}), \tag{50}$$

$$L_k^{v1} - L_k^{v2} \leq 1 + \varepsilon + \bar{M}(1 - \alpha_{1,k}^{v1v2}), \tag{51}$$

$$L_k^{v1} - L_k^{v2} \leq -\varepsilon + \bar{M}(1 - \alpha_{2,k}^{v1v2}), \tag{52}$$

$$L_k^{v1} - L_k^{v2} \geq -1 - \varepsilon - \bar{M}(1 - \alpha_{2,k}^{v1v2}), \tag{53}$$

$$\alpha_{1,k}^{v1v2} + \alpha_{2,k}^{v1v2} = l_{2,k}^{v1v2}, \tag{54}$$

where $\alpha_{1,k}^{v1v2}$ and $\alpha_{2,k}^{v1v2}$ are the 1st and 2nd element of α_k^{v1v2} and ε is a small number. These inequalities ensure that if $L_k^{v1} - L_k^{v2} = 1$, then $\alpha_{1,k}^{v1v2} = 1$ and if $L_k^{v1} - L_k^{v2} = -1$, then $\alpha_{2,k}^{v1v2} = 1$. Also if $L_k^{v1} - L_k^{v2} > 1$ or $L_k^{v1} - L_k^{v2} < -1$, then $\alpha_{1,k}^{v1v2} = \alpha_{2,k}^{v1v2} = 0$. Particularly, (54) ensures that $l_{2,k}^{v1v2} = 1$ only when v1 and v2 are in adjacent lanes.

Based on the relative lane states, the longitudinal maneuvers between the vehicles are designed. The goal of the vehicles in the same lanes is to achieve a safe cruising distance between the consecutive vehicles while the goal of the vehicles in adjacent lanes is to achieve a safe merging distance in this emergency stopping scenario. Let d_s be the longitudinal distance threshold for the same-lane vehicles and d_a be the longitudinal distance threshold for the adjacent-lane vehicles. The safe distance d is calculated as

$$d = \begin{bmatrix} d_s & d_a \end{bmatrix} l_k^{v1v2}. \tag{55}$$

Thus, if the vehicles are in the same lane, $d = d_s$; if the vehicles are in adjacent lanes $d = d_a$; if the vehicles are at least two lanes apart, $d = 0$.

To model the longitudinal coordination of the vehicles, we introduce two binary variables $b_{1,k}^{v1v2}$ and $b_{2,k}^{v1v2}$ and consider the following constraints

$$x_{1,k}^{v1} - x_{1,k}^{v2} \leq -d + \bar{M} b_{1,k}^{v1v2}, \tag{56}$$

$$x_{1,k}^{v1} - x_{1,k}^{v2} \geq d - \bar{M} b_{2,k}^{v1v2}, \tag{57}$$

$$b_{1,k}^{v1v2} + b_{2,k}^{v1v2} \geq 1, \tag{58}$$

where $x_{1,k}$ denotes the longitudinal position and $\bar{M}$ is sufficiently large. When $b_{1,k}^{v1v2} = 0$ and $b_{2,k}^{v1v2} = 1$, (56) becomes $x_{1,k}^{v1} - x_{1,k}^{v2} \leq -d$ and (57) becomes $x_{1,k}^{v1} - x_{1,k}^{v2} \geq d - \bar{M}$, which holds trivially. Similarly, when $b_{1,k}^{v1v2} = 1$ and $b_{2,k}^{v1v2} = 0$, (57) becomes $x_{1,k}^{v1} - x_{1,k}^{v2} \geq d$ and (56) becomes $x_{1,k}^{v1} - x_{1,k}^{v2} \leq -d + \bar{M}$, which holds trivially. Thus, when $b_{1,k}^{v1v2} + b_{2,k}^{v1v2} = 1$, $|x_{1,k}^{v1} - x_{1,k}^{v2}| \geq d$. When $b_{1,k}^{v1v2} = b_{2,k}^{v1v2} = 1$, $d - \bar{M} \leq x_{1,k}^{v1} - x_{1,k}^{v2} \leq -d + \bar{M}$.

For same lane vehicle pairs (i.e., IHV1-AV1, AV2-AV3 in Fig. 3), we enforce the condition $|x_{k,1}^{v1} - x_{k,1}^{v2}| \geq d$ by requiring

$$b_{1,k}^{v1v2} + b_{2,k}^{v1v2} + l_{1,k}^{v1v2} \leq 2 \quad \forall\ k > 1. \tag{59}$$

This condition in conjunction with (56), (57), and (58) ensures that $b_{1,k}^{v1v2} + b_{2,k}^{v1v2} = 1$ for the same lane vehicles, which means they maintain the safe distance d between them. It should be noted that this constraint may not be satisfied for the initial two time steps due to the computational delay and delay in human reaction.

Adjacent lane vehicles do not need to maintain a safe distance from the vehicles in the other lane until it is time to merge. To reduce the time to reach the merging condition between the adjacent lane pairs (e.g., IHV1-AV2, IHV1-AV3, AV1-AV2 in Fig. 3), we introduce a cost function to minimize $b_{1,k}^{v1v2} + b_{2,k}^{v1v2}$ (among other objectives) in the objective function.

For all the vehicles, it is also necessary to model when to change lanes. For a vehicle to change lanes, it must meet the safe distance threshold from vehicles in the adjacent lanes. To ensure this, we introduce the following constraints:

$$b_{1,k}^{v1v2} + b_{2,k}^{v1v2} \leq 1 + [1 - (L_k^{v1} - L_{k+1}^{v1})], \tag{60}$$
$$b_{1,k}^{v1v2} + b_{2,k}^{v1v2} \leq 1 + [1 + (L_k^{v1} - L_{k+1}^{v1})], \tag{61}$$
$$b_{1,k}^{v1v2} + b_{2,k}^{v1v2} \leq 1 + [1 - (L_k^{v2} - L_{k+1}^{v2})], \tag{62}$$
$$b_{1,k}^{v1v2} + b_{2,k}^{v1v2} \leq 1 + [1 + (L_k^{v2} - L_{k+1}^{v2})]. \tag{63}$$

From these constraints, we see that when the lane change takes place, i.e., $L_k^{v1} - L_{k+1}^{v1} = \pm 1$, the condition $b_{1,k}^{v1v2} + b_{2,k}^{v1v2} \leq 1$ must be satisfied. The inequalities (60)–(63) together with (58) enforce that the lane change happens when $b_{1,k}^{v1v2} + b_{2,k}^{v1v2} = 1$ which means that the safe distance d is achieved.

B. Decision variables

We consider an MPC with a look ahead window of K steps. The shared decision variables for each coordinating pair are summarized as $\gamma_k^{v1v2} = [\mathbf{b}_{1,k}^{v1v2}\ \mathbf{b}_{2,k}^{v1v2}\ \mathbf{l}_{1,k}^{v1v2}\ \mathbf{l}_{2,k}^{v2v1}\ \alpha_{1,k}^{v1v2}\ \alpha_{2,k}^{v2v1}]$, where $\mathbf{b}_{1,k}^{v1v2} = \left[b_{1,k}^{v1v2},\ b_{1,k+1}^{v1v2},\ \cdots,\ b_{1,k+K-1}^{v1v2}\right]$, and the other decision variables are defined similarly. For each neighboring pair, the two vehicles have shared coordinating decision variables. Let A_i be the set of adjacent vehicles to vehicle i. Then the full set of shared variables for vehicle i are $\bar{\gamma}_k^i = [\gamma_k^{ij_1} \gamma_k^{ij_2} \ldots]$ where $j_1, j_2, \ldots$ are distinct elements of A_i. The collection of all the $\bar{\gamma}_k^i$ for all the vehicles in the scenario forms the total coordinating decision variable Γ_k. The decision variables for all the AVs, IHVs, and coordinating pairs form the total decision variable denoted by $\theta_k = \{\alpha_k^1, \alpha_k^2, \ldots, \alpha_k^{n^h}, \beta_k^1, \beta_k^2, \ldots, \beta_k^{n^r}, \Gamma_k\}$.

C. Cost function design

The cost function can be designed based on user preferences and the coordination scenario. For our example, we take into account five objectives in the cost function:

1) Minimize the control inputs to the AV and IHV based on their respective weights. This is a quadratic function of θ_k;
2) Maximize the probability of the stochastic events and human input stochasticity. This is a linear function of θ_k;
3) Minimize $b_{1,k} + b_{2,k}$ so that safe distance can be reached quickly. This is a linear function of θ_k;
4) Minimize the number of lane changes. This is a quadratic function of θ_k.
5) Minimize the duration of vehicles in the right lane, encouraging early lane changes. This is a linear function of θ_k.

The objective function of the MPC is the sum of the aforementioned five functions, which can be represented as

$$J(\theta_k) = \theta_k^\top Q \theta_k + c^\top \theta_k, \tag{64}$$

where $Q \in \mathbb{R}^{n_t \times n_t}$ and $c \in \mathbb{R}^{1 \times n_t}$ are the designed objective weights for n_t total decision variables. The $J(\theta_k)$ in (64) is optimized subject to the constraints formulated from the vehicle dynamics in Section IV and the coordination of the vehicles in Section V.

The weights are important factors in designing the best vehicle maneuver as they determine the balance between different objectives and map the control input according to the preferred driving behavior of the user. Like many design problems, these weights are user-defined parameters. Finding an optimal set of weights is of interest but beyond the scope of the paper. Techniques such as inverse reinforcement learning and imitation learning can be leveraged to search for optimal weights given desired user behaviors. In our simulations and experiments, we manually tune the weights to generate reasonable maneuvers and then fix them for evaluation.

VI. Incorporating uncertainty in human's initial state

The human state is a stochastic parameter and may not be determined with full certainty. We can only estimate the human state to a probability. In the initial step $k = 0$, the probability of a human driver following $P(x_0^B = 1)$ and the probability of a human driver's attentiveness $P(a_0 = 1)$ are estimated. The $P(x_0^B = 1)$ is estimated from the driver's pedal data whereas $P(a_0 = 1)$ is estimated from the real-time video of the driver's physical actions. A detailed explanation of the estimation method is provided in our previous work [4]. To estimate the driver's tendency of following advisory commands, we adopt a HMM-based probability model to identify the human driver's actions and then compare them with prior advised actions. Furthermore, we use a residual network (ResNet-50) that recognizes distracted driving behaviors by detecting distinct features from video frames and estimates the probability of human attentiveness. We assume that the two estimated probabilities are independent, resulting in

$$P(s_0^1) = P(a_0 = 0), \tag{65}$$
$$P(s_0^2) = P(a_0 = 1)P(x_0^B = 0), \tag{66}$$
$$P(s_0^3) = P(a_0 = 1)P(x_0^B = 1). \tag{67}$$

To tackle the stochasticity of the human state, we consider three sets of optimization variables that correspond to three possible human states. If the human is in s^1, s^2, or s^3 state, the optimized decision variables are denoted by θ_k^1, θ_k^2 and θ_k^3, respectively. We formulate a combined weighted optimization problem based on the probabilities of each state from (65) to (67) and solve the following optimization

$$\begin{aligned} \min_{\theta_k^1,\theta_k^2,\theta_k^3} \quad & J(\theta_k^1,\theta_k^2,\theta_k^3) = \mathbb{E}_{s_k}\left((\theta_k)^\top Q\theta_k + c^\top\theta_k\right) \\ & = P(s_k^1)\left((\theta_k^1)^\top Q\theta_k^1 + c^\top\theta_k^1\right) \qquad (68) \\ & + P(s_k^2)\left((\theta_k^2)^\top Q\theta_k^2 + c^\top\theta_k^2\right) \\ & + P(s_k^3)\left((\theta_k^3)^\top Q\theta_k^3 + c^\top\theta_k^3\right) \qquad (69) \\ \text{s.t.} \quad & P(s_k^1)\mathbf{G}_k\Big|_{s_k^1=1}\theta_k^1 \le P(s_k^1)\mathbf{g}_k\Big|_{s_k^1=1}, \qquad (70) \\ & P(s_k^2)\mathbf{G}_k\Big|_{s_k^2=1}\theta_k^2 \le P(s_k^2)\mathbf{g}_k\Big|_{s_k^2=1}, \qquad (71) \\ & P(s_k^3)\mathbf{G}_k\Big|_{s_k^3=1}\theta_k^3 \le P(s_k^3)\mathbf{g}_k\Big|_{s_k^3=1}, \qquad (72) \\ & \begin{bmatrix} u_k^r \\ u_k^a \\ u_k^B \end{bmatrix}\Bigg|_{s_k^1=1} = \begin{bmatrix} u_k^r \\ u_k^a \\ u_k^B \end{bmatrix}\Bigg|_{s_k^2=1} = \begin{bmatrix} u_k^r \\ u_k^a \\ u_k^B \end{bmatrix}\Bigg|_{s_k^3=1}, \qquad (73) \end{aligned}$$

where $G_k\theta_k \le g_k$ denotes the accumulated constraints formulating the dynamics and coordination of the vehicles. The constraint (73) ensures that the control inputs to be implemented on the AV and the IHV in the next time step are the same for the three possible states. This is the final sMPC problem which is formulated as a mixed integer optimization problem.

The sMPC solution includes the control inputs to the AVs and the advisory commands conveyed to the IHVs for the next K time steps. The optimal control input for the next time step is applied to the AVs and the optimal advisory commands are announced to the IHVs. At the next time step, the optimization is repeated with the new human state estimates and initial conditions and calculates the optimal input for the next K time steps again. The sMPC solution provides high-level coordinating plans and actions, which are expected to integrate with low-level high-frequency motion planners and controllers.

VII. Simulation results

In this section, we present simulation results and a sensitivity analysis to assess robustness of our approach. A double integrator model is used to simulate vehicle dynamics. The sMPC optimization is solved based on the vehicle states, human input prediction, and human state probability to provide the input for the AV and the advisory command for the IHV. For all simulations, the look-ahead window is $K = 10$ time steps, and each time step is 0.8 seconds. The safe merging distance is $d_s = 10m$ and $d_a = 15m$. The initial velocity of all the vehicles except OBS is set at 14m/s. We have conducted preliminary experiments and observed that average human drivers take 3 steps to change lanes. Thus, we set $f^v = 3$.

We have also conducted an experiment to assess the effect of λ in (14). The experimental result is presented in Section VIII-C. From that experiment, we observe that the use of a tuned λ for a specific driver can improve the performance of the algorithm. However, tuning λ for each driver requires dedicated experiments and collection of sufficient driving data. As we shall see in Section VIII-B, setting $\lambda = 0$ produces satisfactory results in the considered emergency stopping scenario. Thus, we choose $\lambda = 0$ for the simulations and experiments.

The simulations were run in Python on a PC equipped with an Intel(R) Core i9-14900F CPU @ 2.00GHz, 32GB RAM, and an NVIDIA GeForce RTX 4070 Ti SUPER graphics card. To solve the sMPC optimization, we use the Gurobi solver [36]. The computational time for the optimization varies in different scenarios and is below 0.5 sec on average.

A. Emergency stopping simulation

In this section, we present the simulation results of the emergency-stopping scenario shown in Fig. 4 to assess the effectiveness of our formulation. The OBS is simulated to suddenly stop on the right lane of the road. The connected IHV and AVs coordinate to avoid the OBS and maneuver safely in this emergency scenario.

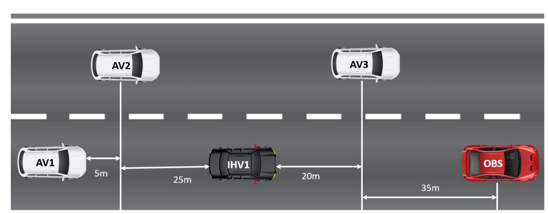

Fig. 4. The simulated emergency stopping scenario: the initial distances and lane configuration.

One set of simulation results is presented in Fig. 5, which shows the simulated coordination maneuvers of the vehicles in the considered scenario. Fig. 5(a) shows the positions and the velocities of each vehicle at each time instant, where dashed and solid lines indicate that the vehicle is in the right and the left lanes, respectively, Fig. 5(b) shows which lane each vehicle is in at each time instant, and Fig. 5(c) illustrates the longitudinal and lane advising commands for the IHV. From the longitudinal advising of the IHV in (c), we observe that the IHV is advised to slow down initially to avoid collision with the OBS. From the lane advising of the IHV, the human driver is advised to change lane for the initial 3 time steps. The subplot (b) illustrates that at the 4th time step, the IHV shifts lanes and moves to the left lane after the lane change advisory. After that, as shown in (c), the IHV is advised to speed up in the longitudinal advising. The AV maneuvers are shown in the subplot (a). AV2 and AV3 are in the left lane so they speed up and create adequate gaps for the other vehicles. Since AV1 is in the right lane, it slows down first and then changes the lane. After changing lanes at the 4th time step, it maintains the speed. The coordinating behaviors of the vehicles demonstrate that our method is able to produce proper and effective control inputs and lane change commands in this emergency stopping scenario.

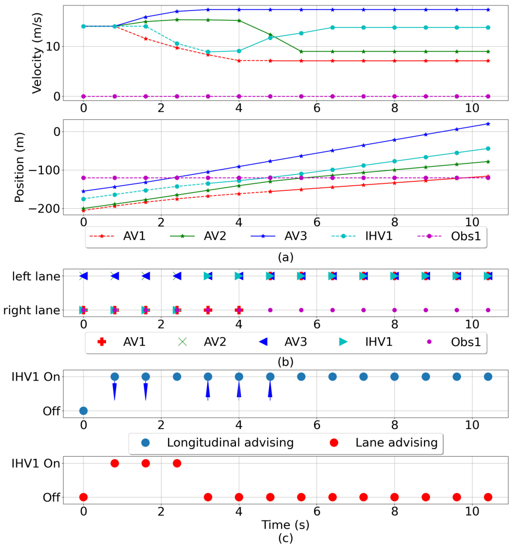

Fig. 5. Simulation results for the emergency stopping scenario. (a) The longitudinal positions and velocities of the vehicles where the dashed line indicates vehicles on the right lane and the solid line indicates vehicles on the left lane. (b) The discrete lane state of the vehicles, and c) Longitudinal and lane advising to the IHV. Upwards, downward arrows, and no arrow indicate 'speed-up', 'slow-down', and 'keep speed' advising actions, respectively.

B. Sensitivity analysis

Our algorithm requires the transition probabilities of the stochastic events. Such probabilities are never known exactly. We conduct a sensitivity analysis to assess the effect of these parameters. This analysis measures how the accuracy of the transition probabilities affects the optimization outcomes for cooperative driving. We focus on a vehicle coordination scenario involving 3 AVs and 1 IHV without the OBS, as shown in Fig. 6. Their initial speed is 14m/s.

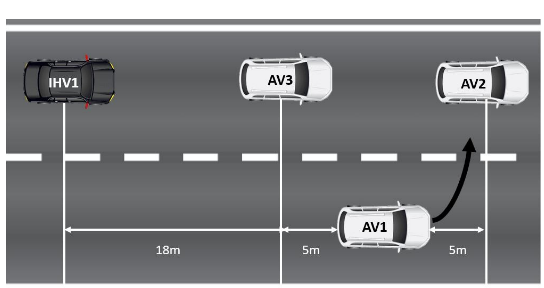

Fig. 6. Initial relative positions of the vehicles for the sensitivity analysis.

We consider multiple setups where the assumed human transition probabilities have errors and are different from the true transition probabilities. We compare the performance with the setup where the transition probabilities are correctly known. We especially examine the control inputs to the different vehicles. Specifically, we consider the transition probability table in Table I below.

TABLE I
HUMAN STATE TRANSITION PROBABILITIES

		$P(s^1_{k+1}=1)$	$P(s^2_{k+1}=1)$	$P(s^3_{k+1}=1)$
$u^B_k=1$	$s^1_k=1$	$P(t^1_k)=0.1$	$P(t^2_k)=0.1$	$P(t^3_k)=0.8$
	$s^2_k=1$	$P(t^4_k)=0.1$	$P(t^5_k)=0.1$	$P(t^6_k)=0.8$
	$s^3_k=1$	$P(t^7_k)=0.1$	$P(t^8_k)=P_a$	$P(t^9_k)=P_b$
$u^B_k=0$	$s^1_k=1$	$P(\bar{t}^1_k)=0.5$	$P(\bar{t}^2_k)=0.5$	$P(\bar{t}^3_k)=0$
	$s^2_k=1$	$P(\bar{t}^4_k)=0.5$	$P(\bar{t}^5_k)=0.5$	$P(\bar{t}^6_k)=0$
	$s^3_k=1$	$P(\bar{t}^7_k)=0.5$	$P(\bar{t}^8_k)=0.5$	$P(\bar{t}^9_k)=0$

We vary P_a and P_b in the following five setups:

1) $P_a=0.1$ and $P_b=0.8$,
2) $P_a=0.275$ and $P_b=0.625$,
3) $P_a=0.45$ and $P_b=0.45$,
4) $P_a=0.625$ and $P_b=0.275$,
5) $P_a=0.8$ and $P_b=0.1$.

We consider the true human model as Setup 1 and the assumed human model for the optimization as Setup 2–5 with increasing error in the transition probabilities P_a and P_b. We conduct 50 Monte Carlo simulations to assess the performance of the optimization and compare it with the optimization results assuming the accurate transition model (Setup 1). In particular, for each setup 2–5, we compare the optimized inputs to different vehicles and calculate the input RMSE (root mean squared error) as

$$I_{RMSE}=\sqrt{\frac{\sum_{k=1}^{T}(I^c_k-I^i_k)^2}{T}} \tag{74}$$

where I^c_k is the optimized input for the correct transition model (i.e., Setup 1), I^i_k is the optimized input for an incorrect transition model (i.e., Setup 2–5) at the k^{th} time step, and I_{RMSE} is the input RMSE over the total merging time T.

Fig. 7 shows the boxplot of the input RMSE of the four vehicles over the 50 Monte Carlo simulations for varying errors in the transition probabilities. The input RMSE statistics of the IHV are similar for different setups because human action always follows the true transition model. However, from the statistics of the AVs, we observe that the input RMSE is low for Setups 2 and 3. If the transition probabilities are significantly different from the true model, such as in Setups 4 and 5, the input RMSE increases significantly in magnitude. Thus, the optimized inputs are reasonably close to the case with the true transition model if P_a and P_b are set close to their true values. This is because the AVs design their optimized maneuvers considering the human driver's stochastic transition probabilities. In addition, the decision to advise the human driver or not is the deciding factor for the optimal AV inputs. Because this decision is discrete, it can tolerate a certain level of inaccuracy in the transition parameters.

VIII. EXPERIMENTAL RESULTS

A. Overview of the cooperative driving platform

The cooperative driving testbed comprises of 1) an IHV which consists of a driving simulator and a user interface in

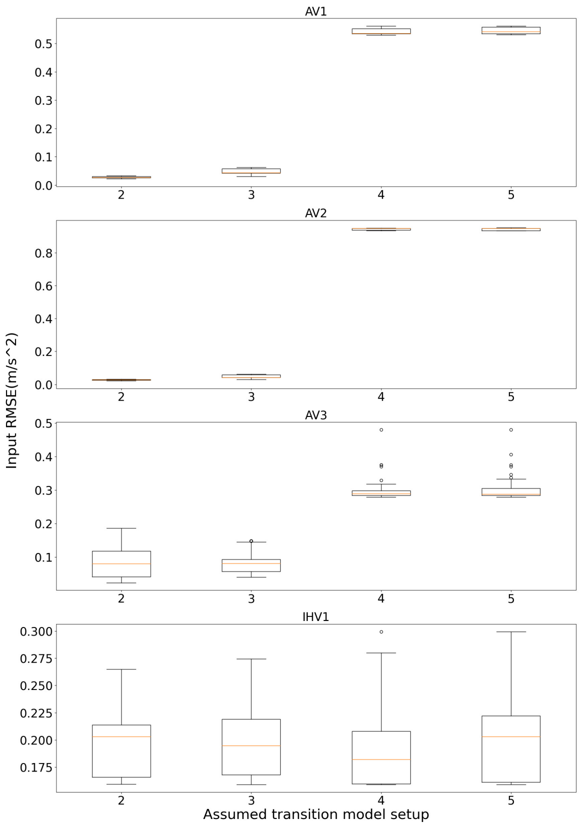

Fig. 7. Boxplots of RMSE of input velocities for different vehicles from 50 Monte Carlo simulations with different P_a and P_b (Setups 2–5). The RMSE is obtained by comparing the velocities from Setup 2–5 (inaccurate models) to the velocities in Setup 1 (true model). The horizontal axis corresponds to Setup 2–5.

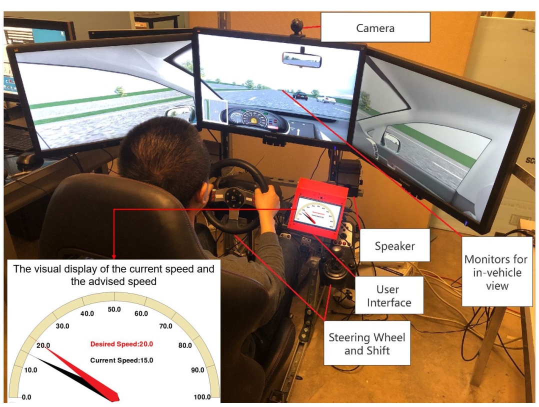

Fig. 8. The cooperative driving simulation testbed.

the form of a copilot, and 2) multiple AVs and OBS running in the driving simulator. As shown in Fig. 8, the driving simulator includes a Logitech G290 driving force suit, which includes a steering wheel, pedals, a gear shifter, and three interconnected monitors for in-vehicle viewing, as well as an additional monitor for data control and observations. The Carnetsoft driving simulator [37] offers an open platform and features a road map database, a script language, an interface to other devices, and user-friendly configuration tools. This driving simulator enables the control of vehicles and the retrieval of their data.

Equipped with a visual display that features a circular chart showing the current speed and advised speed, a speaker, a camera, and a microphone, a user interface is implemented using a Raspberry Pi 4B that manages the interface and communication functions, and an NVIDIA Jetson Nano that performs machine learning and computational tasks.

In the experiment, the distraction detection inference model is executed on the Jetson Nano, while the sMPC model and the driving action recognition model run on a remote desktop computer specified in the simulation results section VII. The computational time for the optimization in the experiments is below 0.8 sec on average including the communication time. The Raspberry Pi acts as a back-end component that receives vehicle data from the driving simulator. It communicates with the Jetson Nano to query the driver's attentiveness and with the remote computer for inputs and outputs. The Raspberry Pi sends control commands back to the simulator for the AVs and provides advice to the human driver through both audio and visual cues. A detailed description of the simulation testbed can be found in [38].

B. Human-in-the-loop emergency stopping experiments

To measure the effectiveness of our developed method, we conduct HITL experiments with human driver volunteers having proficient driving experience. We design three setups for the experiments to simulate varying levels of vehicle coordination and assess the humans' performance under different conditions in the emergency stopping scenario. These setups are designed as follows.

- Setup 1 (collaboration-on and advising-on): In this setup, the system considers the AVs and the IHV as connected vehicles and generates optimal longitudinal and lane inputs for the AVs and the optimal longitudinal and lane advisory for the IHVs considering the human's state estimation and transition model. This setup simulates the scenario where the AVs and the IHV collaborate with direct control inputs and advisory directives to guide the human driver. We use the human state transition probabilities from Table III in Appendix A where the probability of transitioning to the attentive-following state $P(s^3_{k+1} = 1)$ is high when the human driver is advised.
- Setup 2 (collaboration-on and advising-off): In this setup, the system considers the AVs and the IHV as connected vehicles but turns off the advisory inputs to the IHV. The IHV is considered a non-collaborative but connected vehicle. The system generates optimal longitudinal and lane inputs for the surrounding AVs. This setup simulates a scenario where the IHV provides no advisory to the driver but the surrounding vehicles collaborate with each other to maneuver around the non-collaborative IHV. We use the human state transition probabilities from Table IV in Appendix A where the probability of transitioning to the attentive-not-following state $P(s^2_{k+1} = 1)$ is high.
- Setup 3 (collaboration-off and advising-off): In this setup, the system considers the AVs and the IHV as unconnected vehicles. Like Setup 2, the IHV does not provide any

advisory commands. The surrounding AVs do not collaborate to modify the maneuvers but rather keep a constant speed and change lanes at a certain time if it is necessary to avoid the OBS. This setup simulates a scenario where none of the vehicles collaborate and the IHV provides no advisory to guide the driver. We consider this setup as a baseline method and compare the performance of Setup 1 and 2 with this setup.

The three setups are tested with 5 different drivers, each driver repeating each setup 5 times. There are a total of 25 tests for each setup. The AV inputs and the IHV advisory commands are updated every 0.8 seconds based on the optimization from sMPC. In Setup 1, when given an advising command, the copilot announces ‘speed up’, ‘slow down’, or ‘keep’ to influence the human to speed up, slow down, or keep speed, respectively. Also, the copilot announces ‘change lane’ to influence the human to change lanes. As the purpose of this experiment is to test an emergency scenario, the experiment is specifically designed such that participants have little preconception of the experiment conditions. The obstacle vehicle either appears suddenly or comes to a stop suddenly at a random time. The volunteers were unaware of the setup of the experiment so they had no prior knowledge of how the coordination would happen.

We consider one experiment a success if the vehicles avoid the obstacle without collisions in that experiment. In Fig. 9, we show a successful experiment trial for the three setups. From Fig. 9, the difference between the three setups can be analyzed. The human driver is advised in Setup 1 whereas Setup 2 does not announce the advising (see Fig. 9(i)(c) and (ii)(c)). In both setups, the AVs collaborate with the human driver to avoid the stopped OBS. Comparing Setup 1 and 2, we see that both setups are capable of avoiding the OBS. In Setup 2 even though the advisory is turned off, the AVs were able to collaborate, considering the non-following state of the IHV. Setup 3 does not have vehicle collaboration and the IHV does not have any advisory. The AVs have a constant speed while the IHV merge to the left lane at the 3rd time step and then slows down slightly (see Fig. 9(iii)(a)). This successful merge in Setup 3 is one of the very few successful attempts.

Table II shows the number of collisions between the vehicles for the three setups. With Setup 1, there were no collisions between the IHV and the OBS while there were two collisions for Setup 2 and five collisions for Setup 3. Between the IHV and the AVs, there were no collisions for both Setup 1 and Setup 2 while there were collisions for Setup 3. This indicates that the coordination in Setup 1 and 2 is effective in reducing the chances of collisions whether the advising is on or off. However, turning on the advisory (Setup 1) is the most effective in reducing collisions.

The overall performance of the three setups over the 25 experiments is shown in Fig. 10, where the data from the successful experiments for each setup are averaged. From Fig. 10(a), the median distances between the IHV and the OBS in the three setups indicate that on average, Setup 1 has the largest distance of merging. The variances indicate that Setup 1 has the lowest variation of the distances among all the setups, which suggests more consistent performance offered

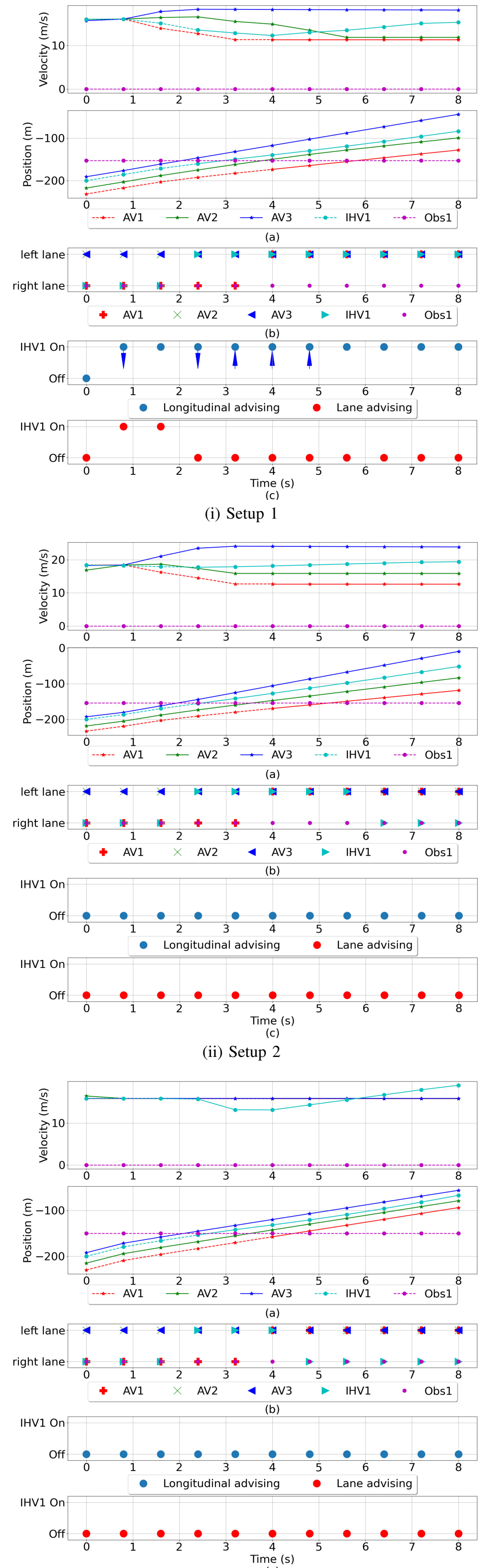

(i) Setup 1

(ii) Setup 2

(iii) Setup 3

Fig. 9. One set of the HITL experimental results for the three setups.

TABLE II
EMERGENCY STOPPING EXPERIMENTS: COLLISIONS

Collisions	**Setup 1**	**Setup 2**	**Setup 3**
between IHV-OBS	0	2	5
between IHV-AV1	0	0	1
between IHV-AV2	0	0	1
between IHV-AV3	0	0	0
Total	0	2	7
Overall success rate	100%	92% (23/25)	72% (18/25)

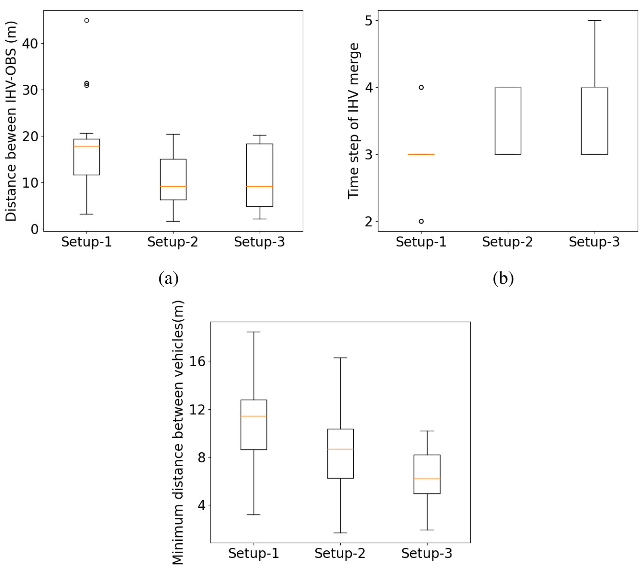

(c)

Fig. 10. Boxplots of (a) the distance between the IHV and the obstacle at the time of merging, (b) the number of time steps that the IHV takes to merge, and (c) the minimum distance between any adjacent vehicles (including OBS) in the same lane in the emergency stopping experiments.

by the proposed cooperative driving method. From Fig. 10(b), the medians of the numbers of time steps taken to complete the merge in the three setups indicate that Setup 1 initiates the merge faster than the other setups. Due to the advisory directives, the IHV in Setup 1 mostly changes lanes at time step 3. Overall, Setup 1 produces safer maneuvers and enables a human driver to respond faster in this emergency-stopping scenario. Fig. 10(c) shows the minimum distances between any adjacent vehicles in the same lane. The median of Setup 1 is the highest, followed by Setup 2 and 3, which indicates that the coordination method helps reduce the chances of close merges between the vehicles.

These experimental statistics validate the performance of the developed method in relevant driving scenarios with multiple vehicles and indicate that cooperative driving with advisory can enable faster reaction of the human driver and reduce the chances of collisions. We have also conducted experiments with $f^v = 0$, i.e., assuming instantaneous lane changes. Since drivers take time to switch lanes, we observed more collisions for Setup 1 and Setup 2. Thus, the lane advisory constraints in (27)–(30) effectively reduce the chances of collisions in this emergency stopping scenario.

C. Effect of λ in the emergency stopping scenario

To analyze the effect of the longitudinal reaction constant λ in (14), we have conducted an experiment to optimize λ, where the human driver's responses to advisory commands were collected. Specifically, we advised a driver to cruise at a specified speed. After the driver was at a steady speed, he/she was advised to 'speed up' or 'slow down' with a specific step input advisory. We conducted this experiment for a range of control input advisories and collected the vehicle's data. Using these data, we computed a λ_t that minimizes the squared error between the IHV's velocity predicted from (14) and the recorded IHV's velocity for all the advisories. For the participating driver, the optimized λ was obtained as $\lambda_t = 0.414$.

For the same driver, we conducted the emergency stopping experiment in Setup 1 with $\lambda = \lambda_t$ and with $\lambda = 0$. The driver repeats the experiment 10 times for each λ. The number of collisions between the vehicles for the two λ settings was zero, which indicates that with the advisory, both settings were successful in avoiding collisions. It also implies that the IHV's lateral motion plays the most vital role in avoiding collisions in this scenario.

In Fig. 11, we compare the two λ settings over the 10 experiments in terms of the merging distance between the IHV and the OBS, the number of time steps that the IHV takes to merge, and the minimum distances between any adjacent vehicle pair in the same lane. We observe from Fig. 11(a) that the median merging distance is higher for $\lambda = \lambda_t$ than for $\lambda = 0$. Fig. 11(b) indicates that setting $\lambda = \lambda_t$ allows the merges to initiate one time step faster than setting $\lambda = 0$. Overall, using the optimized λ_t improves the performance of the algorithm. In Fig. 11(c), even though the median is higher for $\lambda = 0$, the minimum and the first quartile are higher for $\lambda = \lambda_t$, which suggests that setting $\lambda = \lambda_t$ can reduce closer merges and thus enhance safety in the experiments.

IX. CONCLUSIONS AND FUTURE WORK

We present an sMPC formulation for cooperative driving between AVs and IHVs considering the longitudinal and lateral lane states. This formulation incorporates human states, such as attentiveness and the tendency to obey advising directions, while coordinating the motion of IHVs and AVs for optimal maneuvers. The sMPC approach accounts for the stochasticity of human actions to provide optimal AV inputs and advisory instructions for the IHVs. This formulation is capable of generating optimal decisions on the longitudinal and lane control for both AVs and IHVs. Using simulations and experiments in an emergency stopping scenario, we demonstrate that the formulation is effective in reducing the number of collisions and enabling earlier response from the human driver. Our future work involves optimal weight tuning of the objective functions and speeding up the optimization with machine learning and distributed computation.

APPENDIX

REFERENCES

[1] "Autonomous Vehicle Sales Forecast 2018 - AutoTechInsight," [Online; accessed 2022-11-23]. [Online].

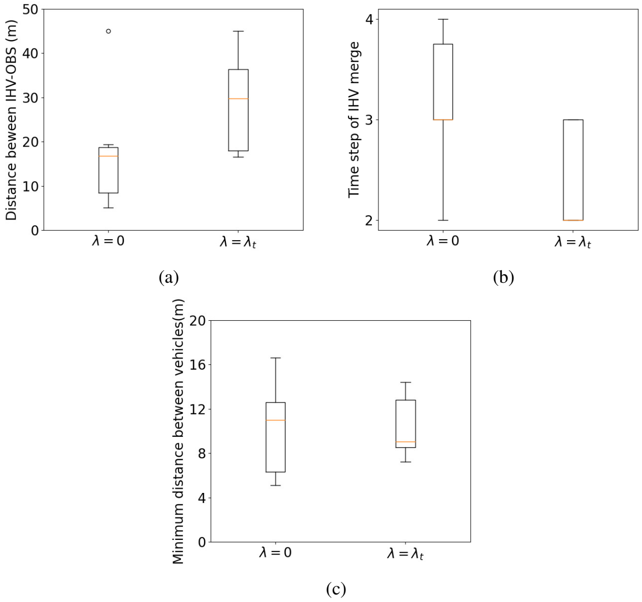

Fig. 11. Boxplots of (a) the distance between the IHV and the obstacle at the time of merging, (b) the number of time steps that the IHV takes to merge, and (c) the minimum distance between any adjacent vehicles (including OBS) in the same lane in the λ optimization experiments.

TABLE III
HUMAN STATE TRANSITION PROBABILITIES FOR SETUP 1

		$P(s_{k+1}^1 = 1)$	$P(s_{k+1}^2 = 1)$	$P(s_{k+1}^3 = 1)$
$u_k^B = 1$	$s_k^1 = 1$	$P(t_k^1) = 0.45$	$P(t_k^2) = 0.05$	$P(t_k^3) = 0.5$
	$s_k^2 = 1$	$P(t_k^4) = 0.2$	$P(t_k^5) = 0.1$	$P(t_k^6) = 0.7$
	$s_k^3 = 1$	$P(t_k^7) = 0.1$	$P(t_k^8) = 0.1$	$P(t_k^9) = 0.8$
$u_k^B = 0$	$s_k^1 = 1$	$P(\bar{t}_k^1) = 0.5$	$P(\bar{t}_k^2) = 0.5$	$P(\bar{t}_k^3) = 0$
	$s_k^2 = 1$	$P(\bar{t}_k^4) = 0.5$	$P(\bar{t}_k^5) = 0.5$	$P(\bar{t}_k^6) = 0$
	$s_k^3 = 1$	$P(\bar{t}_k^7) = 0.5$	$P(\bar{t}_k^8) = 0.5$	$P(\bar{t}_k^9) = 0$

Available: https://autotechinsight.ihsmarkit.com/shop/product/5001816/autonomous-vehicle-sales-forecast-2018

[2] A. Bemporad and S. Di Cairano, "Model-predictive control of discrete hybrid stochastic automata," *IEEE Transactions on Automatic Control*, vol. 56, no. 6, pp. 1307–1321, 2010.

[3] S. Hossain, J. Lu, H. Bai, and W. Sheng, "Stochastic model predictive control for coordination of autonomous and human-driven vehicles," *IFAC-PapersOnLine*, vol. 55, no. 41, pp. 142–147, 2022, 4th IFAC Workshop on Cyber-Physical and Human Systems CPHS 2022. [Online]. Available: https://www.sciencedirect.com/science/article/pii/S2405896323001246

[4] J. Lu, S. Hossain, W. Sheng, and H. Bai, "Cooperative driving in mixed traffic of manned and unmanned vehicles based on human driving behavior understanding," in *2023 IEEE International Conference on Robotics and Automation (ICRA)*, 2023, pp. 3532–3538.

TABLE IV
HUMAN STATE TRANSITION PROBABILITIES FOR SETUP 2

		$P(s_{k+1}^1 = 1)$	$P(s_{k+1}^2 = 1)$	$P(s_{k+1}^3 = 1)$
$u_k^B = 1$	$s_k^1 = 1$	$P(t_k^1) = 0.45$	$P(t_k^2) = 0.5$	$P(t_k^3) = 0.05$
	$s_k^2 = 1$	$P(t_k^4) = 0.2$	$P(t_k^5) = 0.7$	$P(t_k^6) = 0.1$
	$s_k^3 = 1$	$P(t_k^7) = 0.1$	$P(t_k^8) = 0.8$	$P(t_k^9) = 0.1$
$u_k^B = 0$	$s_k^1 = 1$	$P(\bar{t}_k^1) = 0.05$	$P(\bar{t}_k^2) = 0.95$	$P(\bar{t}_k^3) = 0$
	$s_k^2 = 1$	$P(\bar{t}_k^4) = 0.05$	$P(\bar{t}_k^5) = 0.95$	$P(\bar{t}_k^6) = 0$
	$s_k^3 = 1$	$P(\bar{t}_k^7) = 0.05$	$P(\bar{t}_k^8) = 0.95$	$P(\bar{t}_k^9) = 0$

[5] S. Hossain, J. Lu, H. Bai, and W. Sheng, "Incorporating stochastic human driving states in cooperative driving between a human-driven vehicle and an autonomous vehicle," in *2023 IEEE/RSJ International Conference on Intelligent Robots and Systems (IROS)*. IEEE, 2023, pp. 685–690.

[6] ——, "Cooperative driving between autonomous vehicles and human-driven vehicles considering stochastic human input and system delay," in *2023 European Control Conference (ECC)*, 2023, pp. 1–6.

[7] C.-P. Lam, A. Y. Yang, K. Driggs-Campbell, R. Bajcsy, and S. S. Sastry, "Improving human-in-the-loop decision making in multi-mode driver assistance systems using hidden mode stochastic hybrid systems," in *2015 IEEE/RSJ International Conference on Intelligent Robots and Systems (IROS)*, 2015, pp. 5776–5783.

[8] C.-P. Lam and S. S. Sastry, "A POMDP framework for human-in-the-loop system," in *53rd IEEE Conference on Decision and Control*, 2014, pp. 6031–6036.

[9] C. C. Macadam, "Understanding and modeling the human driver," *Vehicle system dynamics*, vol. 40, no. 1-3, pp. 101–134, 2003.

[10] H. Guo, Y. Ji, T. Qu, and H. Chen, "Understanding and modeling the human driver behavior based on mpc," *IFAC Proceedings Volumes*, vol. 46, no. 21, pp. 133–138, 2013.

[11] S. Schnelle, J. Wang, R. Jagacinski, and H. jun Su, "A feedforward and feedback integrated lateral and longitudinal driver model for personalized advanced driver assistance systems," *Mechatronics*, vol. 50, pp. 177–188, 2018. [Online]. Available: https://www.sciencedirect.com/science/article/pii/S0957415818300291

[12] J. Wang, Z. Jiang, and Y. V. Pant, "Improving safety in mixed traffic: A learning-based model predictive control for autonomous and human-driven vehicle platooning," *Knowledge-Based Systems*, vol. 293, p. 111673, 2024.

[13] K. Driggs-Campbell, V. Shia, and R. Bajcsy, "Improved driver modeling for human-in-the-loop vehicular control," in *2015 IEEE International Conference on Robotics and Automation (ICRA)*, 2015, pp. 1654–1661.

[14] S. Chen, H. Yao, F. Qiao, Y. Ma, Y. Wu, and J. Lu, "Vehicles driving behavior recognition based on transfer learning," *Expert Systems with Applications*, vol. 213, p. 119254, 2023.

[15] X. Huang, A. Jasour, M. Deyo, A. Hofmann, and B. C. Williams, "Hybrid risk-aware conditional planning with applications in autonomous vehicles," in *2018 IEEE Conference on Decision and Control (CDC)*. IEEE, 2018, pp. 3608–3614.

[16] R. Tian, L. Sun, A. Bajcsy, M. Tomizuka, and A. D. Dragan, "Safety assurances for human-robot interaction via confidence-aware game-theoretic human models," *ArXiv*, vol. abs/2109.14700, 2021.

[17] Y. Yu, X. Luo, Q. Su, and W. Peng, "A dynamic lane-changing decision and trajectory planning model of autonomous vehicles under mixed autonomous vehicle and human-driven vehicle environment," *Physica A: Statistical Mechanics and its Applications*, vol. 609, p. 128361, 2023.

[18] L. Sun, Z. Cheng, D. Kong, Y. Xu, S. Wen, and K. Zhang, "Modeling and analysis of human-machine mixed traffic flow considering the influence of the trust level toward autonomous vehicles," *Simulation modelling practice and theory*, vol. 125, p. 102741, 2023.

[19] Y. Li, S. Zhang, Y. Pan, B. Zhou, and Y. Peng, "Exploring the stability and capacity characteristics of mixed traffic flow with autonomous and human-driven vehicles considering aggressive driving," *Journal of Advanced Transportation*, vol. 2023, no. 1, p. 2578690, 2023.

[20] D. A. Lazar, R. Pedarsani, K. Chandrasekher, and D. Sadigh, "Maximizing road capacity using cars that influence people," in *2018 IEEE Conference on Decision and Control (CDC)*. IEEE, 2018, pp. 1801–1808.

[21] R. Zhang, S. Masoud, and N. Masoud, "Impact of autonomous vehicles on the car-following behavior of human drivers," *Journal of transportation engineering, Part A: Systems*, vol. 149, no. 3, p. 04022152, 2023.

[22] V. Milanés, J. Pérez, E. Onieva, and C. González, "Controller for urban intersections based on wireless communications and fuzzy logic," *IEEE Transactions on Intelligent Transportation Systems*, vol. 11, no. 1, pp. 243–248, 2009.

[23] L. F. Vismari, J. B. Camargo, J. K. Naufal, J. R. de Almeida, C. B. Molina, R. Inam, E. Fersman, and M. V. Marquezini, "A fuzzy logic, risk-based autonomous vehicle control approach and its impacts on road transportation safety," in *2018 IEEE International Conference on Vehicular Electronics and Safety (ICVES)*. IEEE, 2018, pp. 1–7.

[24] K. Mattas, G. Botzoris, and B. Papadopoulos, "Safety aware fuzzy longitudinal controller for automated vehicles," *Journal of traffic and transportation engineering (English edition)*, vol. 8, no. 4, pp. 568–581, 2021.

[25] H. Li and S. Zhang, "Lane change behavior with uncertainty and fuzziness for human driving vehicles and its simulation in mixed traffic,"

Physica A: Statistical Mechanics and its Applications, vol. 606, p. 128130, 2022.

[26] W. Zhou, D. Chen, J. Yan, Z. Li, H. Yin, and W. Ge, "Multi-agent reinforcement learning for cooperative lane changing of connected and autonomous vehicles in mixed traffic," *Autonomous Intelligent Systems*, vol. 2, no. 1, pp. 1–11, 2022.

[27] L.-y. Zhang, J. Sun, J. Ma, S.-c. Xu, X.-f. Hu, Z.-x. Li, J.-Z. Tang, and Y. Wen, "Simulation study on ramp inflow for hybrid autonomous driving," *Physical Communication*, vol. 55, p. 101932, 2022.

[28] S. Mosharafian and J. M. Velni, "Cooperative adaptive cruise control in a mixed-autonomy traffic system: A hybrid stochastic predictive approach incorporating lane change," *IEEE Transactions on Vehicular Technology*, pp. 1–13, 2022.

[29] B.-K. Xiong, R. Jiang, and X. Li, "Managing merging from a cav lane to a human-driven vehicle lane considering the uncertainty of human driving," *Transportation research part C: emerging technologies*, vol. 142, p. 103775, 2022.

[30] B. Chen, D. Sun, J. Zhou, W. Wong, and Z. Ding, "A future intelligent traffic system with mixed autonomous vehicles and human-driven vehicles," *Information Sciences*, vol. 529, pp. 59–72, 2020.

[31] X. Li, Y. Xiao, X. Zhao, X. Ma, and X. Wang, "Modeling mixed traffic flows of human-driving vehicles and connected and autonomous vehicles considering human drivers' cognitive characteristics and driving behavior interaction," *Physica A: Statistical Mechanics and its Applications*, vol. 609, p. 128368, 2023.

[32] M. Amirgholy and M. Nourinejad, "Connected automated vehicles orchestrating human-driven vehicles: Optimizing traffic speed and density in urban networks," *Transportation Research Part C: Emerging Technologies*, vol. 165, p. 104741, 2024.

[33] S. Mosharafian and J. M. Velni, "A hybrid stochastic model predictive design approach for cooperative adaptive cruise control in connected vehicle applications," *Control Engineering Practice*, vol. 130, p. 105383, 2023.

[34] H. N. Mahjoub, M. Davoodi, Y. P. Fallah, and J. M. Velni, "A stochastic hybrid structure for predicting disturbances in mixed automated and human-driven vehicular scenarios," *IFAC-PapersOnLine*, vol. 51, no. 34, pp. 400–402, 2019.

[35] W. Hoult and D. J. Cole, "A neuromuscular model featuring co-activation for use in driver simulation," *Vehicle System Dynamics*, vol. 46, no. S1, pp. 175–189, 2008.

[36] Gurobi Optimization, LLC, "Gurobi Optimizer Reference Manual," 2022. [Online]. Available: https://www.gurobi.com

[37] Carnetsoft Inc., "Research driving simulator," online : http://www.carnetsoft.com/research-simulator.html.

[38] J. Lu, R. Stracener, W. Sheng, H. Bai, and S. Hossain, "Development of a research testbed for cooperative driving in mixed traffic of human-driven and autonomous vehicles," in *2022 IEEE/RSJ International Conference on Intelligent Robots and Systems (IROS)*, 2022, pp. 11 403–11 408.

Sanzida Hossain (Student Member, IEEE) completed her B.Sc. in Mechanical Engineering in 2016 from the Military Institute of Science and Technology, Bangladesh and her M.Sc. in Mechanical Engineering from Kansas State University, USA in 2020. She is currently pursuing her doctoral degree in Mechanical Engineering at the Mechanical and Aerospace Engineering Department of Oklahoma State University, USA. Her research is focused on cooperative driving between autonomous vehicles and human-driven vehicles in a connected environment considering the stochasticity of human driver behavior.

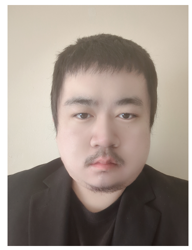

Jiaxing Lu (Student Member, IEEE) received his M.S degree in Computer Science from Stevens Institute of Technology in 2019, and B.S degree in Computer Science from Nanjing University of Aeronautics and Astronautics, Nanjing, China, in 2016. He is currently pursuing the doctoral degree in Electrical Engineering with the Laboratory for Advanced Sensing, Computation and Control (ASCC), Oklahoma State University. His research interest includes cooperative driving in mixed traffic with both autonomous vehicles and human-driven vehicles, as well as modeling and advising human drivers in such HITL systems.

He Bai (Member, IEEE) received his B.S. degree in Automation from the University of Science and Technology of China in 2005, and the M.S. and Ph.D. degrees in Electrical Engineering from Rensselaer Polytechnic Institute in 2007 and 2009, respectively. From 2009 to 2010, he was a Post-doctoral Researcher at Northwestern University. From 2010 to 2015, he was a Senior Research and Development Scientist at UtopiaCompression Corporation. In 2015, he joined the School of Mechanical and Aerospace Engineering at Oklahoma State University, where he is currently an associate professor. His research interests include multi-agent systems, autonomous vehicles, human-robot systems, nonlinear estimation and control, and machine learning.

Weihua Sheng (Senior Member, IEEE) is currently a professor at the School of Electrical and Computer Engineering, Oklahoma State University (OSU), USA. He is the Director of the Laboratory for Advanced Sensing, Computation and Control (ASCC Lab, http://ascclab.org) at OSU. Dr. Sheng received his Ph.D degree in Electrical and Computer Engineering from Michigan State University in May 2002. He obtained his M.S and B.S. degrees in Electrical Engineering from Zhejiang University, China in 1997 and 1994, respectively. He is the author of more than 250 peer-reviewed papers in major journals and international conferences. Eight of them have won best paper or best student paper awards in major international conferences. His current research interests include social robotics, wearable computing, human robot interaction and intelligent transportation systems. His research has been supported by US National Science Foundation (NSF), Oklahoma Transportation Center (OTC) /Department of Transportation (DoT), etc. Dr. Sheng served as an Associate Editor for IEEE Transactions on Automation Science and Engineering and Associate Editor for IEEE Robotics and Automation Magazine.